

CHEMICAL CHARACTERIZATION OF AEROSOL PARTICLES BY
LASER RAMAN SPECTROSCOPY

K. H. Fung and I. N. Tang
Environmental Chemistry Division
Department of Applied Science
Brookhaven National Laboratory
Upton, NY 11973-5000

December 1999
[Original Manuscript Date: September 1995]

To be published in
Aerosol Chemical Processes in the Environment,
Chapter 8, CRC Press LLC, Boca Raton, 2000.
(in press)

By acceptance of this article, the publisher and/or recipient acknowledges the U.S. Government's right to retain a nonexclusive, royalty-free license in and to any copyright covering this paper.

This research was performed under the auspices of the U.S. Department of Energy under Contract No. DE-AC02-98CH10886.

8 Chemical Characterization of Aerosol Particles by Laser Raman Spectroscopy

K.H. Fung and Ignatius N. Tang

CONTENTS

Introduction	
Experimental Techniques	
Laser Sources	
Sample Generation and Illumination	
Collection Optics, Spectrometers, and Detectors	
Current Advances in Chemical Analyses of Aerosol Particles	
Characterization and Identification	
Quantitative Analyses	
Resonance Raman Spectroscopy	
Future Development and Summary	
References	

INTRODUCTION

The importance of aerosol particles in many branches of science, such as atmospheric chemistry, combustion, interfacial science, and material processing, has been steadily growing during the past decades. One of the unique properties of these particles is the very high surface-to-volume ratios, thus making them readily serve as centers for gas-phase condensation and heterogeneous reactions. These particles must be characterized by size, shape, physical state, and chemical composition. Traditionally, optical elastic scattering has been applied to obtain the physical properties of these particle (e.g., particle size, size distribution, and particle density). These physical properties are particularly important in atmospheric science as they govern the distribution and transport of atmospheric aerosols.

The chemical characterization of airborne particles has always been tedious and difficult. It involves many steps in the process, namely, sample collection, species and/or size separation, and chemical analysis. There is a great need for non-invasive methods for *in situ* chemical analysis of suspended single particles. For bulk samples, Raman scattering fluorescence emission, and infrared absorption are the most common spectroscopic techniques. While fluorescence spectroscopy is extremely sensitive in terms of detection limit,¹ it lacks the spectral specificity required for chemical speciation. Furthermore, this technique can only be used for materials that fluoresce in the visible region and, therefore, is quite limited as an analytical tool for general application. Infrared spectroscopy has successfully been applied to chemical characterization of the organic and inorganic

species in size-segregated aerosol samples collected on impactor plates.² Deposited single particles can also be analyzed by infrared microscopy.³ On the other hand, although Arnold and co-workers⁴⁻⁷ have obtained infrared spectra of levitated single aqueous droplets, the infrared absorption of the species is not directly measured in the experiment. Instead, the Mie scattering from the droplet is monitored and the size change due to evaporation as a result of infrared absorption is detected. The experiment is interesting but rather involved. It is difficult to adapt this technique to routine particle analysis because it requires the particle to be spherical in shape and to change size by evaporation during infrared absorption.

Despite the inherent low scattering cross-section of the spontaneous Raman scattering process, Raman spectroscopy has been used rather successfully in particle analysis. In contrast to fluorescence emission and infrared absorption techniques, Raman scattering can be applied to optically opaque, irregular-shaped samples. It is also ideally suited for microscopic samples as well. Moreover, it delivers rich vibrational molecular information that is comparable to infrared spectroscopy for identification purposes. The use of the Raman microprobe is a well-established method for analyzing samples collected on a substrate. Early work in this research area was led by Rosasco and co-workers.⁸⁻¹² Aerosol particles were collected on a filter substrate at first. Then the sample was illuminated by a high-power laser. Various type of compounds, such as inorganic minerals and carbonaceous materials, were analyzed by this technique. Adar and co-workers^{13,14} have subsequently developed a highly automated micro/macroRaman spectrometer. The sensitivity and signal-to-noise ratio of the instrument are high enough to enable a spatial resolution of one micron.

However, there was still a lack of suitable measurement techniques for *in situ* chemical characterization of a levitated particle containing only about 10^{12} molecules. Thurn and Kiefer,^{15,16} in an effort to develop a microprobe technique for suspended particles, have obtained Raman spectra of optically levitated glass particles. The optical levitation of a particle was first demonstrated by Ashkin and Dziedzic.¹⁷ This is, in essence, a turning point for the application of Raman spectroscopy in aerosol research.¹⁸⁻²⁵ Raman spectroscopy of aerosol particles has several interesting properties that are of special interest to aerosol science. The morphology-dependent optical resonances that occur in the Mie scattering of dielectric spheres can interact with the Raman scattered photons. This interaction leads to two physical processes. At the low energy field regime, the simple Mie resonance can interfere and sometimes mask the Raman frequencies.²⁶ The overall inelastic scattered signal can be viewed as a linear summation of the spontaneous Raman scattering and the morphology-dependent Mie resonance. The Mie interference diminishes for larger spheres, as the resonance peaks become lower in amplitude and higher in numbers per spectral bandwidth. At the high energy regime, stimulated Raman emissions can be generated.²⁷⁻²⁹ The Mie resonance peaks provide a high Q-factor for the Raman scattered photons to amplify coherently, and the intensity of the stimulated Raman peaks depend exponentially on the Q-factor of each Mie resonance peak. The stimulated Raman scattering is a nonlinear process, whose intensity is given by

$$I_{sr} = I_s \exp(g_s I_i z), \quad (8.1)$$

where I_s is the spontaneous Raman intensity, g_s is the gain factor, I_i is the incident laser intensity, and z is interaction path length. Mie resonances thus affect the stimulated Raman in two ways. First, the pump path for the laser through the interaction volume is lengthened, typically from the physical size of the particle of a few microns to several meters. The second effect is on the gain factor of the stimulated Raman scattering. This gain factor is proportional to the number density of the Raman active species that are present in the particle. The effective number depends again on the particular Mie resonance peak. Despite the nonlinearity of the intensity in stimulated Raman scattering, some quantitative measurements have been carried out with streams of solution droplets, containing nitrates, sulfates, and phosphates.²⁸⁻³⁰

Resonance Raman scattering is another area of much interest to aerosol characterization. The resonance Raman effect arises when the incident laser frequency is chosen to approach or fall within an absorption band. There are several features that set the resonance Raman scattering technique apart from the spontaneous Raman scattering technique. The most important feature is its capability to probe extremely low concentration samples. However, due to absorption of the incident photons, the sample medium is no longer transparent, resulting in unwanted effects such as fluorescence and heating. In the condensed phase, fluorescence is much reduced by quenching and thus may not constitute an overwhelming problem as it would in the gas phase. Nevertheless, the heating effect is still formidable and this requires special sample-handling techniques for bulk media,³¹ as well as aerosol particles.^{32,33}

This chapter reviews the recent advances in the chemical and physical characterization of suspended single particles by laser Raman spectroscopy. Many of the current experiments outfitted with the state-of-the-art instrumentation are described. Various types of experimental set-ups for aerosol laser Raman spectroscopy are discussed in detail. The detection limits and the analytical applications of the spontaneous Raman and resonance Raman scattering are described and discussed at length. The limitations and future expectations of the Raman techniques in the field of aerosol research are also given.

EXPERIMENTAL TECHNIQUES

A variety of experimental set-ups with different lasers, particle containment chambers, and optical detectors have been used to measure Raman scattering from aerosol particles. It is best to divide the methodologies into two categories. One is the single-particle suspension method and the other is the monodisperse particle stream. These two sampling methods are most frequently used in Raman scattering experiments today.

Although commercial Raman microprobe systems are readily available, many of the aerosol Raman experiments are based on the needs of individual experiments. As a result, only the monochromator and detector components are obtained directly from commercial suppliers without any modifications. In general, an aerosol Raman experiment is designed with specific analytical purpose and the apparatus is built on a modular design basis for maximum flexibility.

LASER SOURCES

Currently, there is a wide range of commercially available lasers suitable for aerosol Raman scattering experiments. For spontaneous Raman scattering, the most frequently used continuous wave (CW) laser is the argon-ion laser. The argon-ion laser typically provides a line-tunable source in the visible and the near-ultraviolet regions. The wavelengths and their relative powers are tabulated in Table 8.1. The argon-ion laser is chosen for aerosol Raman experiments because it has several high-powered laser lines in the blue and green regions of the visible spectrum. Raman emission from these excitation lines fall within the maximum sensitivity region of most optical detectors. Even molecules with very large Raman frequency shifts, such as the OH band in a water molecule (3200 cm^{-1}), can be covered with these optical detectors. In contrast, a krypton-ion laser has nearly as high single-line output powers as the argon-ion laser; however, it has its high-power output lines in the red region (i.e., at 6470.88 \AA and 6764.42 \AA). Consequently, the typical Raman shifted symmetric vibrational bands for the inorganic and OH groups would appear near 7000 \AA and 8200 \AA , respectively, making the krypton laser less desirable. Moreover, the Raman scattering cross-section increases with frequency. Therefore, the blue region in the visible is spectrally most suitable for Raman excitation. For stimulated Raman scattering experiments, the most widely used laser for excitation is the solid-state YAG pulsed laser. The second harmonic line of the YAG laser at 5320 \AA produces a stable and high-power output that is well-suited for stimulated Raman

TABLE 8.1
Spectral Characteristics of
Commonly Used Lasers

Argon-ion laser lines:	
Wavelength (Å)	Relative Intensity
3511.12	0.01
3637.78	0.01
4545.05	0.07
4579.34	0.18
4657.89	0.07
4726.85	0.10
4764.86	0.36
4879.86	0.93
4965.07	0.28
5017.16	0.18
5145.31	1.00
Krypton-ion laser lines:	
Wavelength (Å)	Relative Intensity
5208.31	0.14
5308.65	0.40
5681.88	0.20
6470.88	1.00
6764.42	0.24

scattering. The third harmonic line is less frequently used than the 5320 Å line. The reason for its low popularity is twofold: (1) this line is higher in photon energy and thus increases the possibility of multiphoton ionization, and (2) Rayleigh scattering presents some technical problems because the availability of optical filters for the ultraviolet region is still quite limited.

SAMPLE GENERATION AND ILLUMINATION

The most important consideration for sample containment and illumination is the efficiency of the optical elements involved. The physical dimensions of the particle containment chamber and the vibrating orifice particle generator are usually the determining factors for how the laser beam should be focused when only one laser beam is considered as the sole source for illumination, the minimum focal spot size of the beam for a diffraction-limited beam waist can be easily calculated.³⁴ The spot diameter is given by

$$d_{1/e} = (\pi\lambda/4)(f/D_{1/e}), \quad (8.2)$$

where $d_{1/e}$, $D_{1/e}$, λ , and f are the spot diameter, laser beam diameter, laser wavelength, and focal length, respectively. For a typical argon-ion laser with $D_{1/e} = 2$ mm, at 4880 Å and 10 to 15 cm focal length, the spot diameter is between 20 to 30 μm. Thus, in the laboratory, suspended particles in the 15-μm diameter range can be easily illuminated by this beam. On the other hand, the pulsed YAG laser generates a laser beam with diameter equal to about 9 mm in the second harmonic. Therefore, the corresponding spot size is about 5 to 7 μm.

The most commonly used single-particle containment technique is the quadrupole electrodynamic suspension. A schematic diagram is shown in Figure 8.1. It consists of two dc endcaps and an ac ring electrode. The dc field balances the particle against the gravitational force and the ac

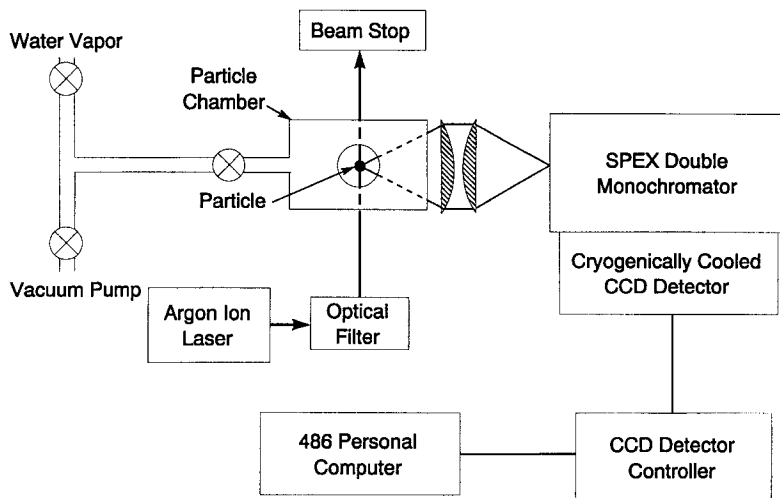


FIGURE 8.1 Schematic diagram of the experimental set-up for single-particle Raman spectroscopy.

field maintains the particle at the center of the cell. A detailed description of the principles is given by Frickel et al.³⁵ Since the introduction of this quadrupole electrodynamic cell concept, there have been several modifications and variations of this design. Davis et al.^{24,25} and Ray et al.³⁶ have used two ac ring electrodes with a dc offset over a glass tube to maximize the collection angle for Raman scattering and fluorescence experiments. Arnold et al.⁶ have used a spherical void design to maximize the light collection efficiency.

In resonance Raman and stimulated Raman experiments, particles no longer suspended in electrodynamic cells. Instead, a stream of droplets are continuously generated by the Berglund-Liu vibrating orifice particle generator.³⁷ This piezoelectric vibrating orifice is made commercially available by TSI (Minneapolis, MN). The feed mechanism in the commercial model consists of a solution reservoir and a syringe pump. The flow rate is found to be uneven when highly monodisperse particles are desired. Snow et al.²⁷ and Lin et al.³⁸ showed that the reservoir can be pressurized by a compressed inert gas such as nitrogen to maintain a steady liquid flow, thus eliminating the use of the syringe pump. In addition, a high throughput, submicron-pore size solution filter can greatly enhance the stability of particle generation.

COLLECTION OPTICS, SPECTROMETERS, AND DETECTORS

The collection optics and spectrometer should always be considered together in aerosol particle Raman scattering experiments. The size of the scattering source is very often the physical diameter of the particle that is imaged onto the entrance slit of the spectrometer. There are two aspects critical for the collection optics that are very important; namely, the magnification of the image and the desired resolution of the Raman spectrum. Assume that the f -numbers of the collection optics and the spectrometer are f_1 and f_2 , respectively. Then, the magnification of the particle image with 100% transmission at the entrance slit would be

$$M = f_2/f_1. \quad (8.3)$$

However, the slit width, which limits the spectrometer resolution, must be set to at least a size of Md in order to transmit the entire particle image (d is the diameter of the particle). Therefore, the larger the particle, the lower the resolution one can obtain for a given dispersion of the spectrometer. On the other hand, the best approach for high resolution in Raman scattering experiments is to use

a spectrometer with high dispersion, which requires the use of both large grating and/or high groove density. This is because the product, Md , is fixed and the resolution of the spectrometer can only be increased by increasing the resolution of the grating.

In practice, Raman experiments require photon-counting techniques that yield the minimum noise level. Although some experiments are still carried out with photomultipliers, most recent experiments are carried out with more efficient detectors, such as the intensified photodiode and charged-coupled device (CCD) array detectors. These modern detectors offer an array approximately 25 mm long. The spatial resolution at the image field is in the vicinity of 22 to 25 μm . Considering the fact that the entrance slit of a typical spectrometer is normally set between 100 and 150 μm to accommodate the image of the aerosol particle, these array detectors thus serve the purpose very effectively. The spectral ranges of these detectors are comparable to those of photomultipliers; they can reach from 250 nm in the ultraviolet to 1100 nm in the infrared. A personal computer is currently a necessity for online control of both the spectrometer and the array detector, as well as for data acquisition and analysis.

There is a major difference between intensified array and non-intensified array detectors. The intensifier resembles a photomultiplier and therefore has intrinsic dark counts. The addition of dark counts due to intensifier limits the exposure time for the array detector. However, the intensifier can be gated, or turned on momentarily in a pulsed laser experiment; hence, the dark counts are substantially reduced. Furthermore, the CCD detector can be cryogenically cooled to the point where the dark count is nearly zero. Therefore, the CCD detectors are extremely well-suited for very low signal level experiments. The CCD detectors have one intrinsic problem: namely, being subject to cosmic ray interference. As a result, the spectra obtained from long-time exposure of CCD arrays always contain numerous random high-intensity spikes due to cosmic rays. These spikes are typically one to two channels in width and can be numerically removed by software routines.

CURRENT ADVANCES IN CHEMICAL ANALYSES OF AEROSOL PARTICLES

The application of laser Raman spectroscopy in the field of aerosol research has steadily grown during the past decade. Although the work published in the literature covers a vast array of topics, it is helpful to categorize them into three general areas that hold special interests for aerosol researchers. These three areas: (1) physical and chemical characterization of aerosol particles, (2) quantitative analyses by Raman spectroscopy, and (3) the development of resonance Raman spectroscopy for aerosol particles.

CHARACTERIZATION AND IDENTIFICATION OF AEROSOL PARTICLES

Aerosol particles of inorganic salts in the crystalline state usually exhibit characteristic Raman frequency shifts with a very narrow bandwidth; whereas, in solution, the corresponding Raman frequency shifts are slightly displaced and the peaks are broadened by molecular motion.^{21,39,40} A typical example is shown in Figure 8.2, where the Raman spectra taken of a sodium nitrate (NaNO_3) particle (a) as a solution droplet, (b) during phase transformation from liquid solution to solid state, and (c) as a crystalline particle, clearly show the changes in the molecular vibrational band features for the same particle in different physical states. The observed Raman shifts at 1051 cm^{-1} for the free nitrate ion (NO_3^-) in aqueous solution droplets and at 1067 cm^{-1} for NaNO_3 crystalline particles are in good agreement with the literature data obtained for bulk samples. The measured linewidth for the droplet is typically 6 cm^{-1} , compared with only 2 cm^{-1} for the solid particle. Thus, the Raman shifts, combined with the large difference in the linewidth between the solid and liquid states, provide a viable means for particle characterization.

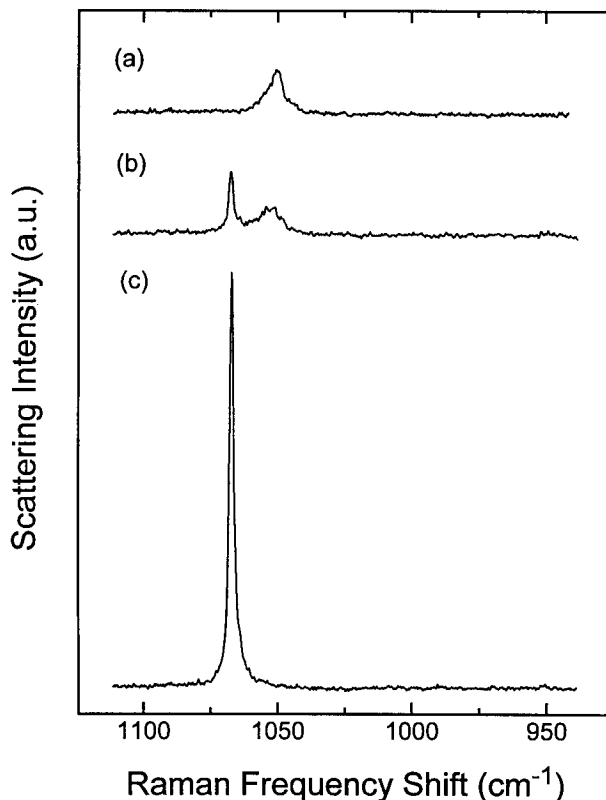


FIGURE 8.2 Raman spectra of an NaNO_3 solution droplet undergoing phase transformation to form a crystalline particle.

Many inorganic salts in the crystalline form can exist either as anhydrous salts or as hydrated salts containing one or more water molecules of crystallization, depending on the chemical nature and the crystallization conditions. Ammonium sulfate is a common constituent of atmospheric aerosols and it always exists in the anhydrous form. In bulk solutions, sodium sulfate crystallizes below 35°C to form the stable hydrated solid, $\text{Na}_2\text{SO}_4 \cdot 10\text{H}_2\text{O}$. Some inorganic salts may have more than one stable hydrated form. Chang and Irish⁴¹ have reported Raman and infrared studies of hexa-, tetra-, and dihydrates of crystalline magnesium nitrate. The latter two hydrates are formed from partial dehydration of the hexahydrate under vacuum at 30 to 40°C . However, given the temperature extremes that can be attained in the atmosphere, most inorganic salts are not expected to exist in more than two different crystalline forms in atmospheric aerosols. For example, magnesium nitrate has two stable hydrated states that are expected to be present in ambient aerosols. At temperatures below -20°C , it exists as $\text{Mg}(\text{NO}_3)_2 \cdot 9\text{H}_2\text{O}$, and above -8°C , it exists as $\text{Mg}(\text{NO}_3)_2 \cdot 6\text{H}_2\text{O}$. These two hydrates may coexist at temperatures between -20 and -8°C . The anhydrous state and other hydrates of magnesium nitrate can only be prepared under conditions that are not encountered in the atmospheric environment.

In order to identify the hydrated or anhydrous forms present in an aerosol particle, it is necessary to have band resolutions better than a few wavenumbers (cm^{-1}). Table 8.2 gives a list of Raman frequencies for several common nitrates and sulfates. The proximity of these Raman vibrations clearly illustrates the need for high-resolution spectrometers for aerosol particle analyses. For example, the presence of anhydrous sodium sulfate (Na_2SO_4) or the hydrated form ($\text{Na}_2\text{SO}_4 \cdot 10\text{H}_2\text{O}$) in aerosol particles can only be confirmed with a minimum resolution of $\pm 1 \text{ cm}^{-1}$, which is needed to identify the corresponding Raman frequencies of 996 cm^{-1} and 992 cm^{-1} , respectively.

TABLE 8.2
Summary of Raman Frequencies (cm⁻¹) Observed for Inorganic Salt Particles

Nitrates		Sulfates		Phosphates	
LiNO ₃	1070	Li ₂ SO ₄ · H ₂ O	1008	Na ₂ HPO ₄	935
LiNO ₃ · 3H ₂ O	1056	Na ₂ SO ₄	996	(NH ₄) ₂ HPO ₄	913
NaNO ₃	1067	Na ₂ SO ₄ · 10H ₂ O	992	NH ₄ H ₂ PO ₄	913
KNO ₃	1053	K ₂ SO ₄	983		
NH ₄ NO ₃	1050	(NH ₄) ₂ SO ₄	975		
Mg(NO ₃) ₂	1064	MgSO ₄ · 7H ₂ O	983		
Mg(NO ₃) ₂ · 6H ₂ O	1059				
Ca(NO ₃) ₂ · 4H ₂ O	1050				
Sr(NO ₃) ₂	1056				
Ba(NO ₃) ₂	1047				
Pb(NO ₃) ₂	1047				
		Solution Droplets		Chromates	
		NO ₃ ⁻	1048	Na ₂ CrO ₄	851
		SO ₄ ²⁻	980	K ₂ CrO ₄	852
		HSO ₄ ⁻	892 1048		
				Mixed Salts	
				Na ₂ SO ₄ · NaNO ₃	996 1063
				(NH ₄) ₂ SO ₄ · NH ₄ NO ₃	975 1043
				NH ₄ HSO ₄	860 1025
				(NH ₄) ₃ HSO ₄	960 1065

Aerosol particles composed of inorganic salts such as chlorides, sulfates, and nitrates are hygroscopic and exhibit the properties of deliquescence and efflorescence in humid air. These aerosols play an important role in many atmospheric processes that affect local air quality, visibility degradation, as well as global climate. The hydration behavior, the oxidation and catalytic capabilities for trace gases, and the optical and radiative properties of the ambient aerosol all depend crucially on the chemical and physical states in which these microparticles exist. The existence of hygroscopic aerosol particles as metastable aqueous droplets at high supersaturation has routinely been observed in the laboratory⁴²⁻⁴⁴; and verified in the ambient atmosphere.⁴⁵ Because of the high degree of supersaturation at which a solution droplet solidifies, a metastable amorphous state often results. The formation of such state is not predicted from bulk-phase thermodynamics and, in some cases, the resulting metastable state is entirely unknown heretofore.⁴⁶ Figure 8.3 shows the hydration behavior of the Sr(NO₃)₂ particle, where the particle mass change resulting from water vapor condensation or evaporation is expressed in moles H₂O per mole solute and plotted as a function of relative humidity (%RH). A crystalline anhydrous particle, whose Raman spectrum shown in Figure 8.4b, displays a narrow peak at 1058 cm⁻¹ and a shoulder at 1055 cm⁻¹, was first subjected to increasing RH (filled circles). The solid particle was seen to deliquesce at 83% RH when it spontaneously gained weight by water vapor condensation and transformed into a solution droplet containing about 13 moles H₂O/ moles solute. Further growth of the droplet, as RH was again increased, was in complete agreement with the curve computed from bulk solution data.⁴⁷ As RH was reduced, the droplet started to lose weight by evaporation (open circles). It remained a supersaturated metastable solution droplet far below the deliquescence point until it abruptly transformed into an amorphous solid particle at ~60% RH. The particle retained some water even in vacuum. The Raman spectrum of such a particle is shown in Figure 8.4d, displaying a broad band at 1053 cm⁻¹, in sharp contrast to those of the anhydrous particle and the bulk solution (Figure 8.4c). In most cases, an amorphous solid particle would continuously absorb a very small amount of water upon increasing RH until they deliquesced at 69% RH. Once in solution, the particle would behave like a typical solution droplet. In the special case shown in Figure 8.3, however, the particle (crosses) was observed to have transformed first into an anhydrous particle during increasing RH and the deliquesced at 83% RH, indicating that the amorphous solid particle was metastable

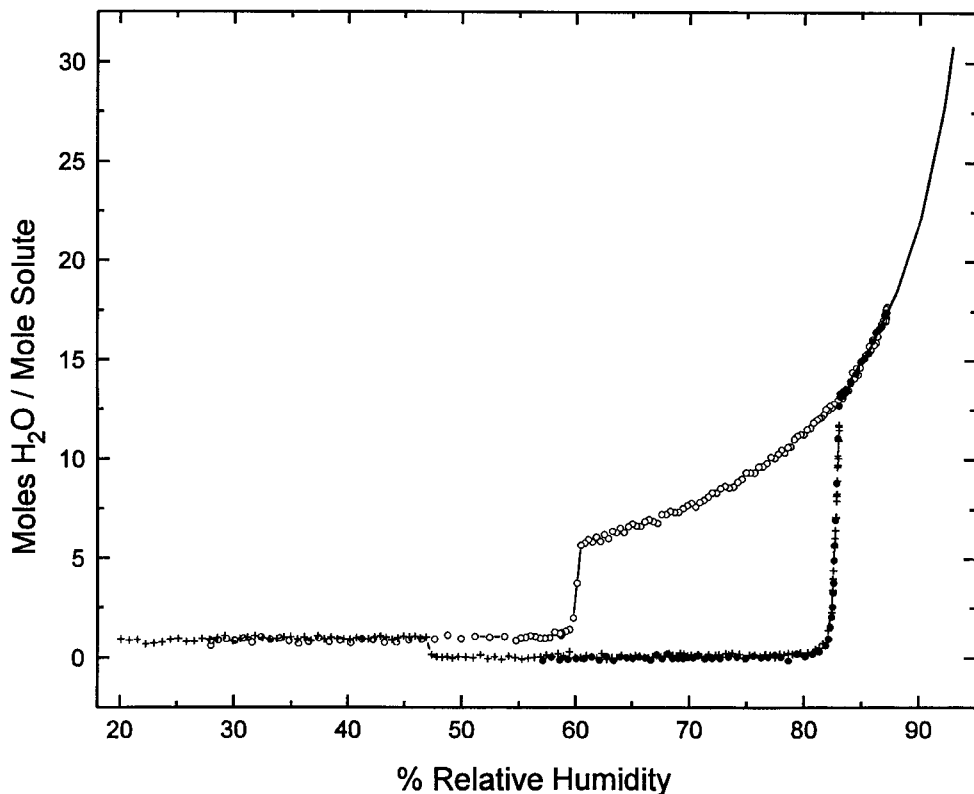


FIGURE 8.3 Growth and evaporation of a suspended $\text{Sr}(\text{NO}_3)_2$ particle in a humid environment: (a) particle growth #1 (\bullet); (b) particle growth #2 ($+$); (c) droplet evaporation (\circ); and, (d) literature data (solid line).

with respect to the anhydrous state. The Raman spectrum of the hydrated $\text{Sr}(\text{NO}_3)_2 \cdot 4\text{H}_2\text{O}$ is shown in Figure 8.4a for comparison. This hydrated form of strontium nitrate is the one that exists in bulk samples, but is not found in particles.

Other nitrate systems such as calcium nitrate and magnesium nitrate also show the formation of amorphous state upon recrystallization of solution droplets. Typically, the water content of these amorphous particles increases slightly with increasing relative humidity. They have a distinctive deliquescence point that is lower than that of their respective crystalline counterparts. In addition to these nitrate systems, metastable states are observed in several bisulfate systems. Figure 8.5b shows a Raman spectrum of ammonium bisulfate, NH_4HSO_4 , in bulk samples. The strongest bisulfate bands are centered at 1013 and at 1041 cm^{-1} . However, the ammonium bisulfate particle shows a completely different spectrum, as shown in Figure 8.5a. The strongest band is no longer split, but centers at 1021 cm^{-1} . All the other spectral features are simpler and slightly shifted as well. It has been proposed⁴⁸ that the bisulfate has two different structures in the crystalline form. As a result, a splitting occurs at the bisulfate vibration bands. When a bisulfate solution droplet recrystallizes at high supersaturation, it is likely that, due to kinetic constraints, only one of the two proposed structures emerges to form the crystalline phase, yielding a Raman spectrum with less vibration bands.

Ambient aerosols are far from being a single-component system. In fact, the chemical composition of atmospheric aerosols is highly complex and may vary considerably with time and location. In solution droplets, the presence of different cations does not appreciably affect the vibration frequencies of the anions that are being monitored by the Raman spectroscopic technique; therefore, the free ions (such as nitrate and sulfate ions) exhibit their characteristic Raman shifts, for all

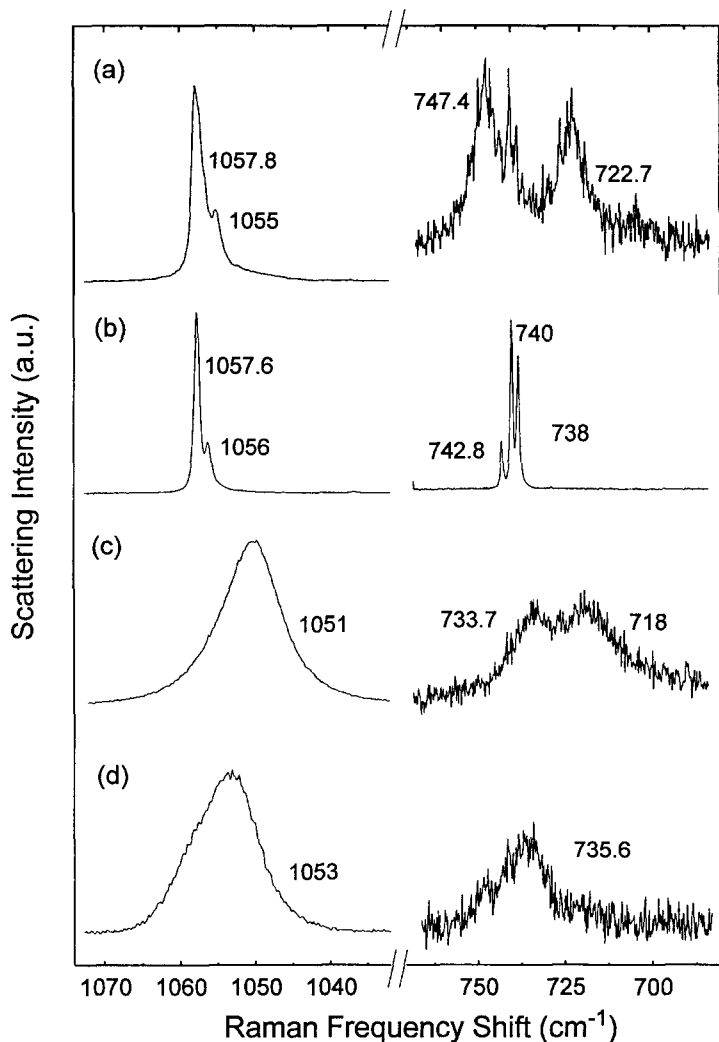


FIGURE 8.4 Raman spectra of $\text{Sr}(\text{NO}_3)_2$ in different physical and chemical states: (a) crystalline $\text{Sr}(\text{NO}_3)_2 \cdot 4\text{H}_2\text{O}$; (b) anhydrous $\text{Sr}(\text{NO}_3)_2$; (c) bulk $\text{Sr}(\text{NO}_3)_2$ aqueous solution; and (d) $\text{Sr}(\text{NO}_3)_2$ particle.

practical purposes, irrespective of the different kinds of cations present in the droplet. However, when a droplet containing multicomponent electrolytes transforms into a solid particle under low humidity conditions, the chemistry and kinetics of the system will operate to govern the outcome of crystallization process.

Thus, for non-interacting systems, the droplet will simply solidify to contain salt mixtures that make up the composition of the original dry-salt particle. For these particles, the composition can be determined from the relative peak intensities and the Raman cross-sections of the respective components. Figure 8.6a shows a Raman spectrum of a potassium nitrate and potassium sulfate solution droplet, indicating only SO_4^{2-} at 980 cm^{-1} and NO_3^- at 1049 cm^{-1} without any information about the cation. The Raman spectrum of the recrystallized solid particle is shown in Figure 8.6b, where the peaks reveal the characteristic Raman shifts of K_2SO_4 at 983 cm^{-1} and KNO_3 at 1053 cm^{-1} . Note that the band broadening effect in the droplet is quite apparent as compared to the crystalline particle.

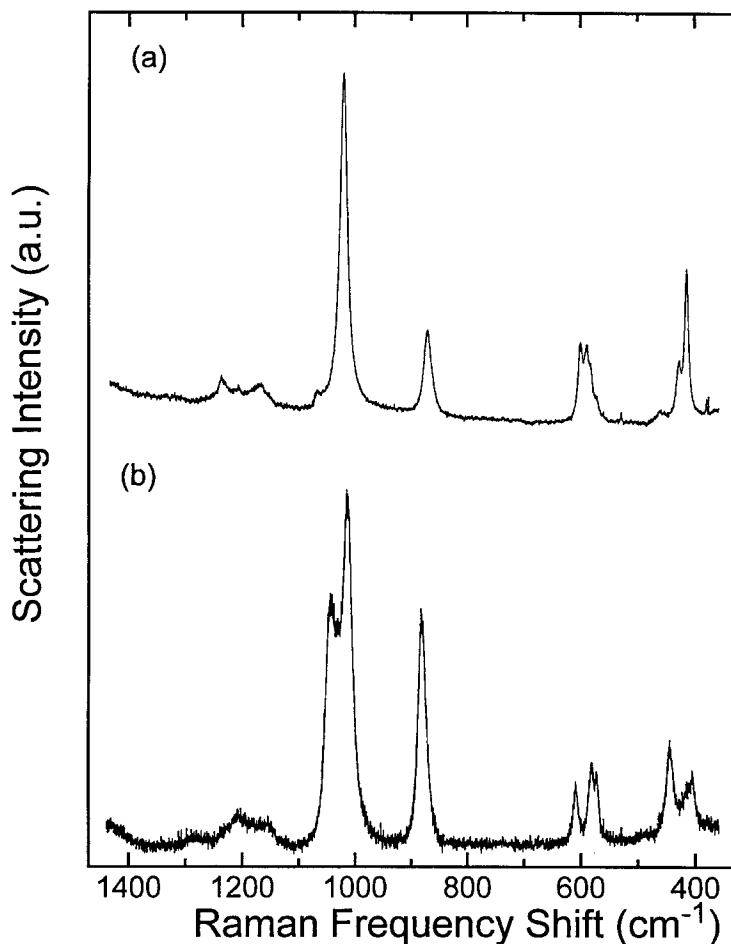


FIGURE 8.5 Raman spectra of NH_4HSO_4 in (a) a particle, and (b) in bulk phase.

However, many inorganic salts upon crystallization from its aqueous solution are known to form mixed salts that are stable stoichiometric compounds. Mixed salts have been shown to be present in ambient aerosols and in laboratory-generated aerosols. The Raman lines of mixed salts may be very different from those of the pure component salts, or they may represent a slight displacement that only becomes apparent with ultra-high spectral resolution. For example, in the crystallization of a solution droplet containing sodium and ammonium cations and sulfate and nitrate anions,³⁹ the solid particle may contain salts of all possible combinations, namely, NH_4NO_3 , $(\text{NH}_4)_2\text{SO}_4$, NaNO_3 , and Na_2SO_4 , which have strong symmetric Raman bands at 1050 cm^{-1} , 975 cm^{-1} , 1067 cm^{-1} and 996 cm^{-1} , respectively (see Table 8.2). In addition, mixed salts can also form.⁴⁹ For example, in the solid particle formed from a solution droplet containing Na_2SO_4 and NaNO_3 (molar ratio 1:4), the Raman spectrum shown in Figure 8.7a reveals the presence of not only the pure components at 1067 cm^{-1} and 996 cm^{-1} , but a new band at 1063 cm^{-1} , which is attributed to the presence of mixed salt $\text{NaNO}_3 \cdot \text{Na}_2\text{SO}_4 \cdot \text{H}_2\text{O}$. Similarly, Figure 8.7b shows the Raman spectrum of a solid particle containing a 1:4 mixture of NaNO_3 and NH_4NO_3 , where a new Raman band observed at 1053 cm^{-1} is attributed to the formation of the mixed salt $2\text{NH}_4\text{NO}_3 \cdot \text{NaNO}_3$. The formation of the mixed crystal in an aerosol particle is largely governed by the kinetic conditions at crystallization. For droplets of identical composition, the outcome of the mixed crystals is not always the same.

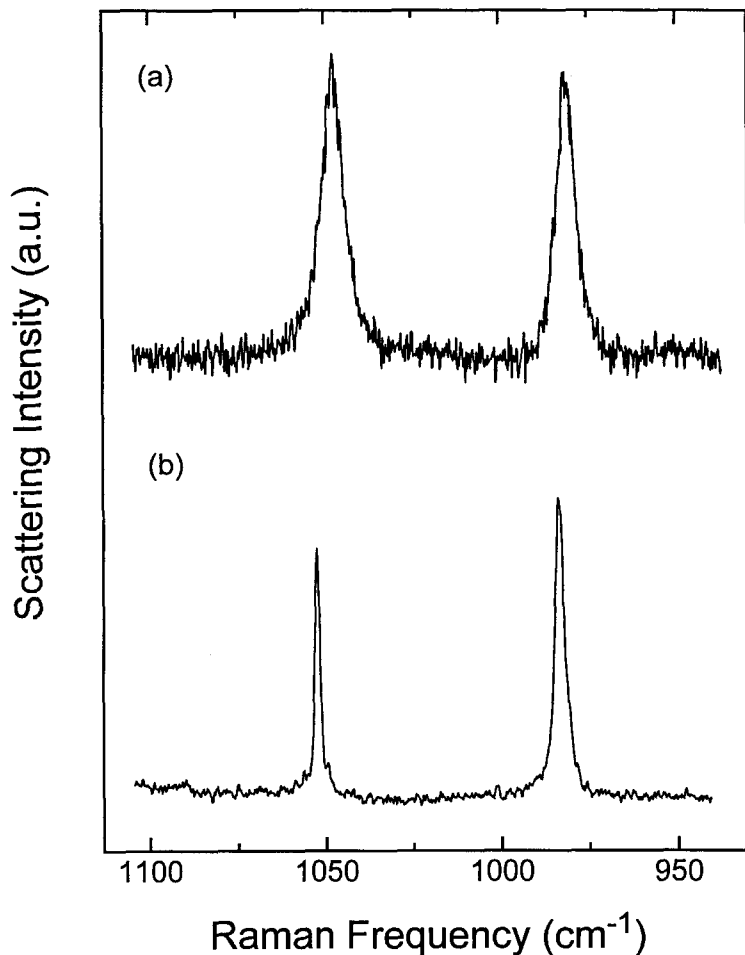


FIGURE 8.6 Raman spectra of a solution droplet containing K_2SO_4 and KNO_3 , (a) before and (b) after crystallization.

QUANTITATIVE ANALYSES

There are several aspects in considering the use of spontaneous Raman scattering as a quantitative measuring technique for aerosol particles. In principle, the Raman scattering intensity, I_s , is proportional to the total number of Raman active scattering molecules or centers, $l\sigma\rho$, and the intensity of the excitation source, I_i :

$$I_s = I_i l \sigma \rho, \quad (8.4)$$

where l is the interaction length, σ is the Raman scattering cross-section, and ρ is the density. However, for aerosol particles, these parameters are extremely difficult to measure in practice. As the size of the particle changes, the number of Raman active scattering molecules or centers will be different, and the overlap between the laser beam and the particle can also vary. Moreover, for solution droplets, the morphology dependent Mie resonances can interfere with and modify the overall Raman scattering intensity. Therefore, it is helpful to have an internal standard for aerosol Raman intensity measurement. This internal standard can easily eliminate the particle size variation

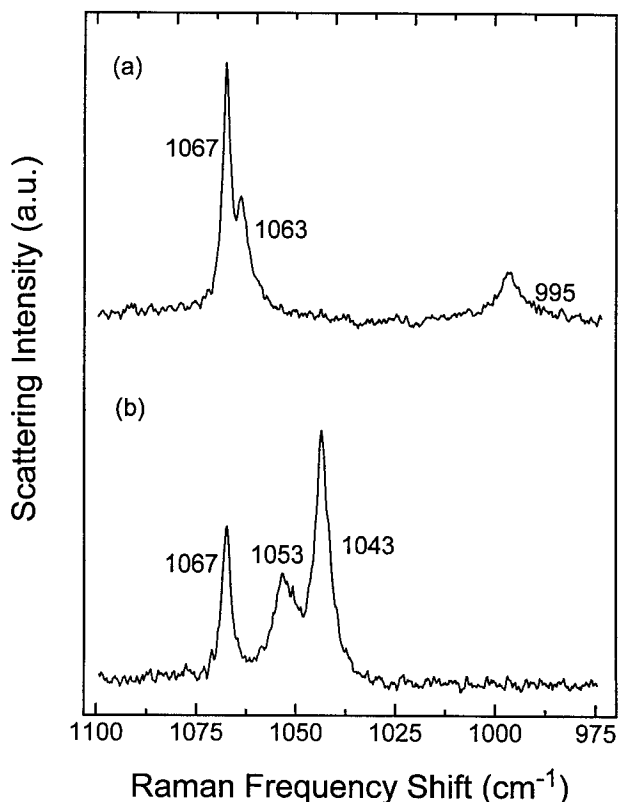


FIGURE 8.7 Raman spectra of multicomponent salt particles showing the presence of mixed salts: (a) 4:1 mixture of NaNO_3 and Na_2SO_4 , and (b) 1:4 mixture of NaNO_3 and NH_4NO_3 .

and the fluctuation in the intensity of the excitation source. In laboratory studies, many non-interacting Raman active species can be added to the samples of interest. For ambient aerosols, water is often a dominant component and can be used as intensity reference.⁵⁰ On a positive note, aerosol particles are physically thin samples. Typically, they are only a few micrometers in diameter. Thus, problems arising from optical diffusiveness as encountered⁵¹ in bulk samples have less effect on aerosol particles.

An example of quantitative measurement is illustrated with the system of ammonium sulfate and sodium sulfate solid mixtures.⁴⁹ A Raman spectrum of an aerosol particle composed of $(\text{NH}_4)_2\text{SO}_4$ and Na_2SO_4 is shown in Figure 8.8. This spectrum represents an exposure of 10 seconds, producing a signal intensity about 6000 counts/s. The peak shape is entirely Lorentian. The symmetric vibrational bands of the two sulfate groups show a small overlap. To account for the proper integrated peak-area signal, the spectrum is computer-resolved and best-fitted with a set of optimal values of peak position and width by a numerical routine. The optimization algorithm follows the nonlinear least-squares method outlined by Marquardt.⁵² In Figure 8.9, a plot of the scattering intensity ratio against the molar mixing ratio of Na_2SO_4 to $(\text{NH}_4)_2\text{SO}_4$ is shown. The linearity of this plot is very good. The slope of the line, which represents the relative Raman cross-section ratio of Na_2SO_4 to $(\text{NH}_4)_2\text{SO}_4$ in this case, is found to be 0.65 ± 0.01 by linear regression analysis. Experimental data points, in general, represent the average results from at least three different aerosol particles; this is to ensure the even distribution of samples. The line width of both sulfate peaks shows a small increase, when compared to that of the pure component form. The slight broadening of the Raman peaks indicates the presence of the solid mixture of the two sulfates.

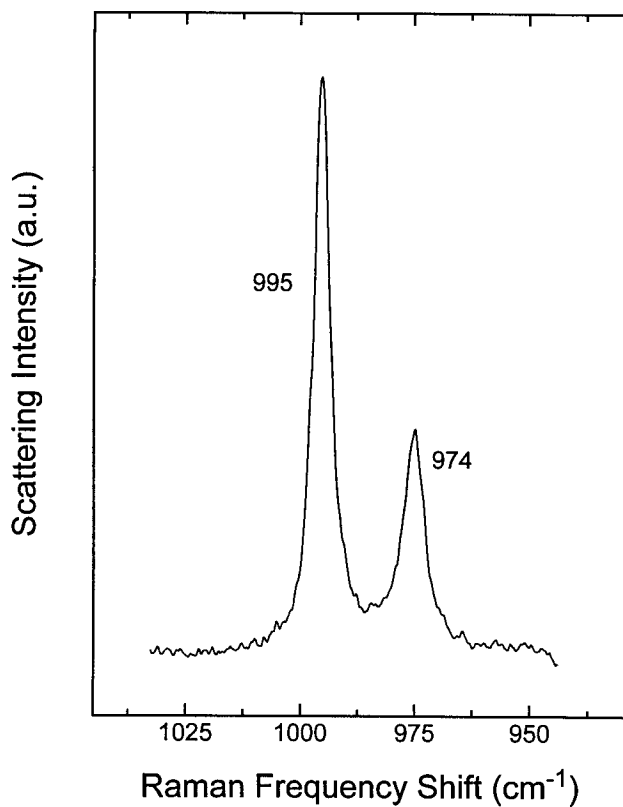


FIGURE 8.8 Raman spectra of a suspended $(\text{NH}_4)_2\text{SO}_4 + \text{Na}_2\text{SO}_4$ (1:4) particle.

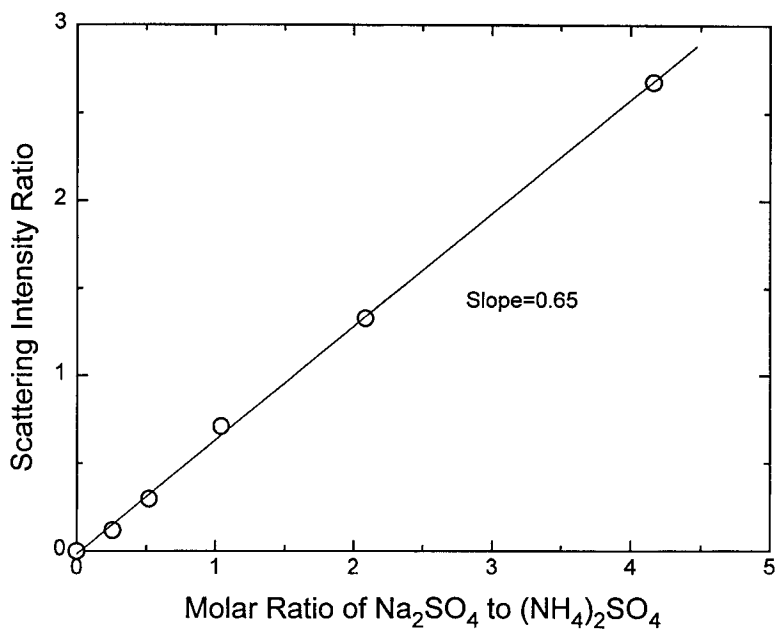


FIGURE 8.9 Dependence of relative Raman intensity on molar ratio of Na_2SO_4 to $(\text{NH}_4)_2\text{SO}_4$ in particles.

The quantitative Raman analysis for microdroplets^{53,54} needs special attention. The morphology-dependent Mie resonances can affect the over-all Raman scattering intensity. The incident intensity is given by

$$I_i = 1/2(e/\mu)^{1/2}|E_1|^2, \quad (8.5)$$

where e is the electric inductive capacity and μ is the magnetic inductive capacity. $|E_1|^2$ is the internal electric field strength due to the incident beam. According to Mie theory, this internal field for spherical particles is different from that for bulk samples. The Raman scattering intensity is linearly proportional to the intensity of the incident radiation:

$$I_s = \text{constant} \times I_i. \quad (8.6)$$

Therefore, the morphology-dependent resonances directly modify the Raman emission from a spherical droplet. In order to compensate for this effect, the best approach is to use an internal standard to correct for this input Mie resonance effect. The Raman scattered photons are also subject to the Mie resonance condition. This output resonance effect can be seen to produce superimposed components on the spontaneous Raman signals.^{15,18}

RESONANCE RAMAN SPECTROSCOPY

As mentioned earlier, the resonance Raman effect arises when the incident laser frequency is tuned to the absorption band of the species of interest. The absorption spectra of the aqueous solutions of sodium dichromate, sodium chromate, potassium permanganate, and *p*-NDMA (*p*-nitrosodimethylaniline) are shown in Figure 8.10.³³ In this example, the excited state of both dichromate and chromate lie outside the range of the wavelengths available in the argon-ion excitation laser. Therefore, the resonance effects can be interpreted as pre-resonance Raman. The absorption band of the *p*-NDMA and the permanganate solutions provides a better overlap with the laser coverage. Thus, they can be considered in the resonance Raman regime. However, the permanganate may be governed by some of the post-resonance effects, as the excitation energy is higher than the maximum of the absorption band.

Due to the pre-resonance Raman effect, the dichromate and chromate ions were found to have cross-sections only about 12 and 10 times larger than that of the nitrate ion, respectively. Here in this study of aerosol particles, the nitrate ion was used as the internal standard, enabling the measurement of relative Raman cross-sections. The permanganate solution shows dominantly post-resonance effects, as the laser energy lies beyond the absorption maximum. A detailed study of this wavelength dependence has been made by Kiefer and Bernstein^{31,55} with bulk solution samples. In droplets, the permanganate ion was found to have its Raman cross-section about 300 times larger than that of the nitrate ion. For *p*-NDMA, there are two strong Raman bands at 1164 cm^{-1} and 1613 cm^{-1} , which are the phenyl-nitroso deformation and symmetric benzene ring-stretching vibrations, respectively. Figure 8.11 shows the Raman spectrum of a solution droplet containing potassium nitrate (0.02 *M*), potassium sulfate (0.02 *M*), and *p*-NDMA (10⁻⁵ *M*). At the 4880 Å excitation wavelength, the measured enhancement for *p*-NDMA with respect to nitrate or sulfate is 3×10^4 . The detection limit in this example is of the order of 10⁻⁷ *M* for *p*-NDMA.³⁰

As is well known, the Mie theory precisely describes the light scattering from spherical particles. The Mie scattering function can be strongly influenced by the imaginary, or the absorption part of the index of refraction. As this imaginary part increases, both the angular scattering intensity distribution and the size scattering intensity, distribution become more monotonic. Effectively, the morphology-dependent peaks are softened by the absorption component and the scattering function

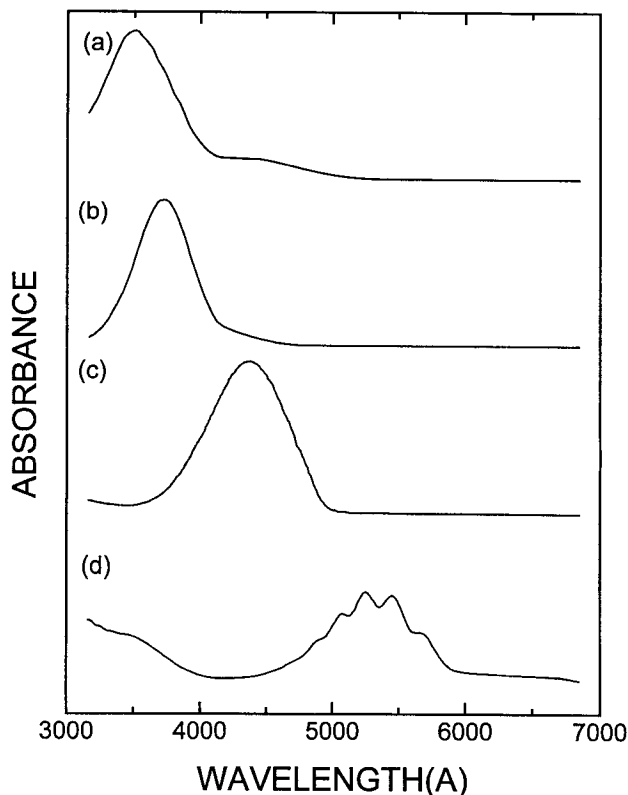


FIGURE 8.10 Absorption spectra of aqueous solutions of (a) sodium dichromate, (b) sodium chromate, (c) *p*-NDMA, and d) potassium permanganate.

approaches the absorption limit of the scattering center. Kerker⁵⁶ has given a detailed discussion as well as graphic illustration of the effects of the imaginary part on the scattering function. Besides the effects of the imaginary part on the Mie scattering function, the variation in the droplet size can also affect the Mie resonances. For example, a 45- μm droplet would have very dense morphology-dependent resonance peaks. Typically, the change in the droplet diameter is about 0.26 μm between adjacent resonance peaks. The large light collection angle (approximately 60°) used in the Raman scattering experiment further reduces this 0.26- μm spacing to 0.12 μm . Meanwhile, the Mie resonance peak width is also broadened, from 0.05 μm to 0.02 μm , by the large light collection angle. Therefore, an estimate of less than 0.1 μm or 0.2% variation in the droplet diameter would sufficiently smooth out most of the Mie resonance features. The absence of the Mie elastic scattering features in the spectra can be attributed to the two factors mentioned above. Even in the event of highly monodisperse droplets, this unique property of resonance Raman spectroscopy can be used to dampen the Mie resonance peaks. Hence, a more meaningful quantitative measurement can be obtained.

Another unique feature in the resonance Raman scattering is the occurrence of a long progression of overtones. From the point of molecular spectroscopy, these overtones allow the determination of anharmonicity in the molecular vibration. Such observation was obtained on solid potassium chromate by Kiefer and Bernstein.⁵⁵ A total of ten harmonics of the internal stretching mode, ν_1 , at 853 cm^{-1} was observed. In addition, only total symmetric vibrations have such characteristics. It was observed that some B symmetry vibrations were absent in the resonance Raman spectrum. In the case of solution droplets, overtones for the permanganate ion were also observed.³² The

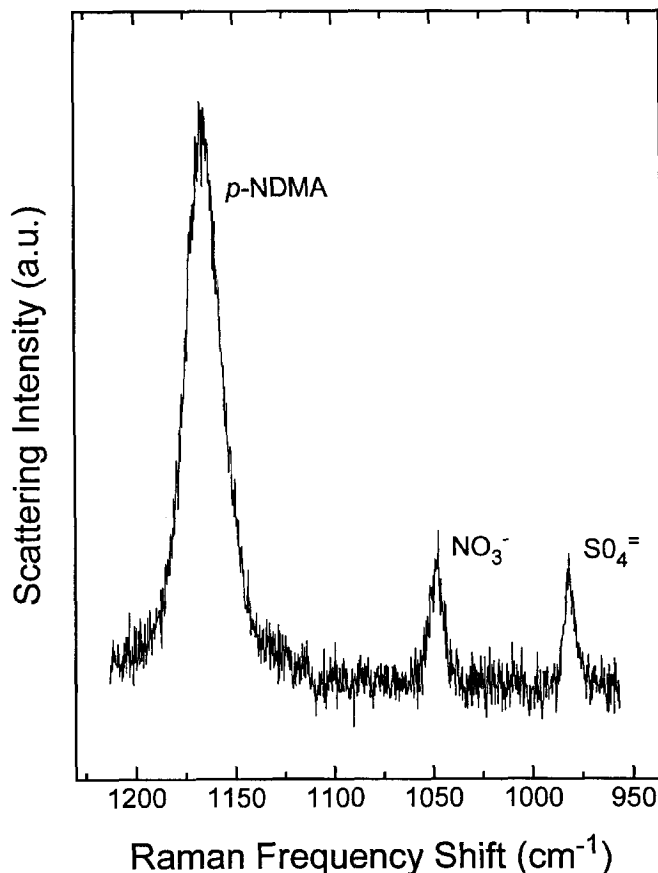


FIGURE 8.11 Raman spectrum of a solution droplet containing potassium nitrate, potassium sulfate, and *p*-NDMA.

progression was limited to a few overtones due to the lack of sensitivity. The anharmonicity obtained from the solution droplet is in good agreement with the one derived from bulk samples.

SUMMARY AND FUTURE DEVELOPMENT

As laser Raman spectroscopy of aerosol particles is only in its infancy, new developments leading toward higher sensitivity and better selectivity for chemical characterization are anticipated. Extraction of information from Mie scattering-affected Raman bands is of particular importance to microdroplet analysis. During the past decade, there have been many advances made in optical instrumentation development, the generation and containment of aerosol particles, and other spectroscopic analytical techniques as well. However, particle Raman spectroscopy has almost become a standard laboratory technique for microparticle research. Current Raman scattering techniques largely focus on the aerosol particle as a whole. Resonance enhancement techniques would allow the investigation of the surface layer coverage of the aerosol particles by selectivity tuning the excitation wavelength to the absorption bands of the species of interest. Since many chemical and physical processes are occurring at the gas-particle interface, an ultimate challenge is to probe and study these surface layers. The resonance Raman technique may emerge as an important tool in this respect.

REFERENCES

1. Barnes, M.D., Whitten, W.B., and Ramsey, J.M., *Anal. Chem.*, 67, 418A, 1995.
2. Allen, D.T., Palen, E.J., Haimov, M.I., Hering, S.V., and Young, J.R., *Aerosol Sci. Technol.*, 21, 325, 1944.
3. Allen, D.T. and Palen, E.J., *J. Aerosol Sci.*, 20, 441, 1989.
4. Arnold, S. and Pluchino, A.B., *Appl. Optics*, 21, 4194, 1982.
5. Arnold, S., Murphy, E.K., and Sageev, G., *Appl. Optics*, 24, 1048, 1985.
6. Arnold, S., Neuman, M., and Pluchino, A.B., *Optics Lett.*, 9, 4, 1984.
7. Sageev-Grader, G., Arnold, S., Flagan, R.C., and Seinfeld, J.H., *J. Chem. Phys.*, 86, 5897, 1987.
8. Rosasco, G.J., Etz, E.S., and Cassatt, W.A., *Appl. Spectrosc.*, 29, 396, 1975.
9. Rosasco, G.J., Roedder, E.R., and Simmons, J.H., *Science*, 190, 557, 1975.
10. Rosasco, G.J. and Blaha, J.J., *Appl. Spectrosc.*, 34, 140, 1980.
11. Blaha, J.J., Rosasco, G.J., and Etz, E.S., *Appl. Spectrosc.*, 32, 292, 1978.
12. Blaha, J.J. and Rosasco, G.J., *Anal. Chem.*, 50, 892, 1978.
13. Grayzel, R., LeClerq, M., Adar, F., Lerner, J., Hutt, M., and Diem, M., *Microbeam Analysis*, Armstrong, J.T., Ed., San Francisco Press, San Francisco, 1985.
14. Adar, F., *ACS Symposium Series*, 295, 230, 1986.
15. Thurn, R. and Kiefer, W., *Appl. Spectrosc.*, 38, 78, 1984.
16. Thurn, R. and Kiefer, W., *Appl. Optics.*, 24, 1515, 1985.
17. Ashkin, A. and Dziedzic, J.M., *Phys. Rev. Lett.*, 38, 1351, 1977.
18. Lettieri, T.R. and Preston, R.E., *Optics Comm.*, 54, 349, 1985.
19. Preston, R.E., Lettieri, T.R., and Semerjian, H.G., *ACS Langmuir J.*, 1, 365, 1985.
20. Schrader, B., *Physical and Chemical Characterization of Individual Airborne Particles* K.R. Spurny, Ed., Chapter 19. Halsted, New York, 1986.
21. Fung, K.H. and Tang, I.N., *Appl. Optics*, 27, 206, 1988.
22. Schweiger, G., *Particle Charact.*, 4, 67, 1987.
23. Schweiger, G., *J. Aerosol Sci.*, 21, 483, 1990.
24. Davis, E.J. and Buehler, M.F., *Mater. Res. Soc. Bull.*, 15, 26, 1990.
25. Davis, E.J., Buehler, M.F., and Ward, T.L., *Rev. Sci. Instrum.*, 61, 1281, 1990.
26. Chew, et al. (1976).
27. Snow, J.B., Qian, S.X., and Chang, R.K., *Opt. Lett.*, 10, 37, 1985.
28. Eickmans, J.H., Qian, S.X., and Chang, R.K., *Part. Charact.*, 4, 85, 1987.
29. Serpengüzel, A., Chen, G. and Chang, R.K., *Part. Sci. Technol.*, 8, 197, 1990.
30. Fung, K.H., Imre, D.G., and Tang, I.N., *J. Aerosol Sci.*, 25, 479, 1994.
31. Kiefer, W. and Bernstein, H.J., *Appl. Spectrosc.*, 25, 609, 1971.
32. Fung, K.H. and Tang, I.N., *J. Aerosol Sci.*, 23, 301, 1992a.
33. Fung, K.H. and Tang, I.N., *Appl. Spectrosc.*, 46, 159, 1992b.
34. Strong, J., *Concepts of Classical Optics*, Freeman, San Francisco, 1958.
35. Frickel, R.H., Schaffer, R.H., and Stamatoff, J.B., *Chamber for the Electrodynamic Containment of Charger Aerosol Particles*, National Technical Information Service Report No. AD/A 056236, U.S. Department of Commerce, Springfield, VA, 1978.
36. Ray, A.K., Souyri, A., Davis, E.J., and Allen, T.M., *Appl. Optics*, 30, 3974, 1991.
37. Berglund, R.N. and Liu, B.Y.H., *Environ. Sci. Technol.*, 7, 147, 1973.
38. Lin, H.-B., Eversole, J.D., and Campillo, A.J., *Rev. Sci. Instrum.*, 61, 1018, 1990.
39. Fung, K.H. and Tang, I.N., *J. Colloid Interface Sci.*, 130, 219, 1989.
40. Tang, I.N. and Fung, K.H., *J. Aerosol Sci.*, 20, 609, 1989.
41. Chang, G.T. and Irish, D.E., *Can. J. Chem.*, 85, 995, 1973.
42. Orr, C., Hurd, F.K., and Corbett, W.J., *J. Colloid Sci.*, 13, 472, 1958.
43. Tang, I.N., Munkelwitz, H.R., and Davis, J.G., *J. Aerosol Sci.*, 8, 149, 1958.
44. Richardson, C.B. and Spann, J.F., *J. Aerosol Sci.*, 15, 563, 1984.
45. Rood, M.J., Shaw, M.A., Larson, T.V., and Covert, D.S., *Nature* 337, 537, 1989.
46. Tang, I.N., Fung, K.H., Imre, D.G., and Munkelwitz, H.R., *Aerosol Sci. Technol.*, 23, 443, 1995.
47. Robinson, R.A., and Stokes, R.H., *Electrolyte Solutions*, 2nd Ed., Butterworth, London, 1970.
48. Payan, F. and Haser, R., *Acta Cryst.* B32, 1875, 1976.

49. Fung, K.H. and Tang, I.N., *Appl. Spectrosc.*, 45, 734, 1991.
50. Chang, C.K., Flagan, R.C., and Seinfeld, J.H., presented at the *1990 American Association for Aerosol Research Annual Meeting*, Philadelphia, PA, 1990.
51. Blomer, F. and Moser, H., *Z. Angew. Phys.*, 5, 302, 1969.
52. Marquardt, D.W., *J. Soc. Industr. Appl. Math.*, 11, 431, 1963.
53. Buehler, M.F., Allen, T.M., and Davis, E.J., *J. Coll. Interface Sci.*, 146, 79, 1991.
54. Buehler, M.F. and Davis, E.J., *Colloids and Surfaces: A Physicochemical and Engineering Aspects*, 79, 137, 1993.
55. Kiefer, W. and Bernstein, H.J., *Molec. Phys.*, 23, 835, 1972.
56. Kerker, M., *The Scattering of Light and Other Electromagnetic Radiation*, Academic Press, New York, 1969.